Dear Author,

Please, note that changes made to the HTML content will be added to the article before publication, but are not reflected in this PDF.

Note also that this file should not be used for submitting corrections.

Materials Science & Engineering A ∎ (∎∎∎∎) ∎∎∎–∎∎∎

Contents lists available at ScienceDirect

Materials Science & Engineering A

journal homepage: www.elsevier.com/locate/msea

Stress–strain response and microstructural evolution of a FeMnCAl TWIP steel during tension–compression tests

J.A. Benito [a,b,*], R. Cobo [a], W. Lei [c], J. Calvo [a,c], J.M. Cabrera [a,c]

[a] Fundació CTM Centre Tecnològic de Manresa, Plaça de la Ciència 2, 08243 Manresa, Spain
[b] Department of Materials Science and Metallurgical Engineering, EUETIB, Universitat Politècnica de Catalunya, Comte d'Urgell 187, 08036 Barcelona, Spain
[c] Department of Materials Science and Metallurgical Engineering, ETSEIB, Universitat Politècnica de Catalunya, Av. Diagonal 647, 08028 Barcelona, Spain

ARTICLE INFO

Article history:
Received 11 June 2015
Received in revised form
15 December 2015
Accepted 2 January 2016

Keywords:
TWIP steels
Bauschinger effect
Mechanical twinning
Dislocation structure

ABSTRACT

The stress–strain response of a Fe–17.5Mn–0.7C–2Al TWIP steel during cyclic loading has been investigated by means of tension–compression tests within the strain limits of ±2%, ±5% and ±10%. In addition, the microstructural evolution during the ±5% cyclic test has also been studied. The difference between the forward and reverse stress for each pre-strain has been analyzed at 0.2% offset strain and at the strains in which forward and reverse curves were parallel in order to study the Bauschinger effect (BE) and permanent softening, respectively. The evolution of the BE with pre-strain for this steel is similar to other FeMnC TWIP steels, that is, increasing values of BE are obtained as the pre-strain increases. However, its absolute values are half those reported in the literature on other FeMnC steels. This diminution of the BE is related to the lower activity of mechanical twinning in FeMnCAl TWIP steels at the pre-strains herein investigated, which promotes less polarized stresses in the matrix due to the lower dislocation storage capacity.

Regarding permanent softening, the evolution is similar to that of the BE and the same analysis can be applied. During reverse compression, a slight increase of twin thickness and twin spacing with respect to the first tensile stage took place. This fact might be linked to the lower flow stress observed in the permanent softening period during reverse straining.

1. Introduction

Twinning-induced plasticity (TWIP) steels are being extensively studied because of their excellent combination of high-tensile strength and large ductility. One of the most promising applications is the manufacture of car components where energy absorption is a determining factor. It is well-known that one of the problems during sheet forming of high strength steels is the large amount of springback.

In the control of springback, numerical methods (such as the finite element method) are used to predict the differences between the final obtainable forms and the designed forms. With this knowledge, die modifications can be carried out and springback can be controlled (and minimized) following an iterative process. In order to obtain accurate forming simulations and therefore diminish the number of iterations, it is necessary to use good plasticity models that can give accurate stress predictions. The hardening law to be introduced in the these models must be able to predict the cyclic stress–strain behavior of the given material, especially when bending–unbending operations are involved, such as the ones taking place in industrial forming processes. It is particularly important to model the reverse loading flow curve, which should include the Bauschinger effect, the transient behavior and the permanent softening [1].

The hardening models that have shown better accuracy in predicting the magnitudes of the forward and reverse stresses are based on mixed isotropic–kinematic hardening laws [2,3]. Kinematic hardening is added to isotropic hardening by the so-called "back stress" that reflects the anisotropy of the yield strength. This back stress causes an increase of stress during forward straining but helps to decrease the flow stress in the opposite direction. This back stress can be determined by different tests: three-point bending tests [1], shear tests [4] and tension–compression tests [5].

Various studies on the cyclic behavior of TWIP steels [6] and on reverse loading [7,8] have been carried out in recent years. In these studies, a Fe–22Mn–0.6C steel was selected, and it was observed a large contribution of the kinematic hardening to the

* Correspondence to: Materials Science Department, Pavelló E. ETSEIB, Av. Diagonal, 647, 08028 Barcelona Spain.
E-mail address: Josep.a.benito@upc.edu (J.A. Benito).

http://dx.doi.org/10.1016/j.msea.2016.01.004
0921-5093/

overall hardening. This large contribution was related to the combined effect of mechanical twins formed during deformation and the glide of dislocations, which are pinned at twin boundaries [9]. The storage of dislocations in the matrix by the action of twin boundaries is in the basis of the stress–strain response of TWIP steels; some hardening models have been proposed to relate these mechanisms to the pronounced work-hardening observed in these steels [10,11].

Despite the excellent tensile properties of FeMnC TWIP steels, it has to be mentioned that some problems have been reported in the literature. Among these problems we can find low yield strength, delayed fracture and heterogeneous deformation. The addition of Al can solve some of these problems since it suppresses the precipitation of cementite [12], promotes solid solution hardening, reduces H-embrittlement related to the delayed fracture and reduces Dynamic Strain Aging (DSA) [13]. On the other hand, FeMnCAl TWIP steels show less mechanical twinning activity and lower strain hardening rates than FeMnC TWIP steels [13–15]. As already mentioned, the development of back stresses in TWIP steels has been related to the combined mechanism between mechanical twins and dislocations glide, so the lower twinning activity of FeMnCAl steels should reflect in lower values of back stress with pre-strain in cyclic tests.

Although the tensile properties and strain hardening of FeMnCAl TWIP steels have been widely studied [13–16] there is very little information about its response in reverse loading. The present study, therefore, investigates the stress–strain behavior and the microstructural evolution of ~~a~~ FeMnCAl TWIP steels during cyclic tests. The possible differences in the evolution of the back stress with increasing strain and its relationship with mechanical twinning could indirectly help to understand the important contribution of kinematic hardening in TWIP steels.

2. Materials and methods

The studied material was a hot rolled TWIP steel sheet provided by POSCO with a thickness of 2.6 mm. The chemical composition in mass percentage is listed in Table 1 and the initial average grain size was 4 μm, although the grain size varied within from 0.6 to 18 μm. The microstructure and the local texture of the initial and deformed material during the 5% strain cycle were characterized by Electron Back Scattered Diffraction (EBSD) on the longitudinal plane, at approximately half thickness. The samples were mechanically polished with 2500 grit SiC paper until down to 0.02 μm colloidal silica suspension following standard metallographic procedures. EBSD measurements were performed using a JEOL JSM-7001 F Field Emission Scanning Electron Microscope (FE SEM) using the Oxford Instruments HKL channel 5 software package. A step size of 0.1 μm was used and misorentations below 3° were not considered in the post processing data procedure. Additional analysis of the microstructure was performed using the Kikuchi pattern quality (KPQ) maps from EBSD scans and standard FE SEM micrographs. Transmission Electron Microscopy (TEM) was carried out to investigate twin thickness and twin spacing as well as the evolution of the dislocation arrangement in the deformed samples. The specimens were analyzed in a Philips CM30 microscope operating at 300 kV. Samples for TEM

Table 1
Chemical composition of the TWIP steel used in this study (in weight percent).

Material	Mn	C	Si	Al	Ti	Mo	Fe
%	17.0	0.73	0.07	1.91	0.10	0.31	Bal.

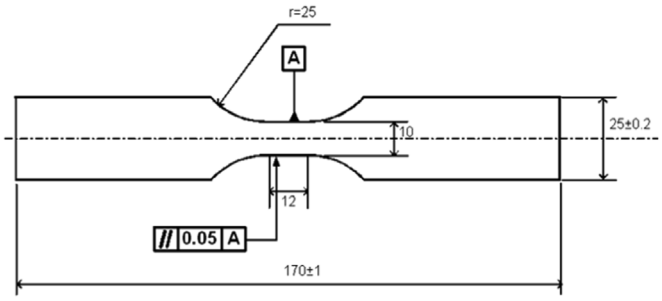

Fig. 1. Dimensions of the samples used for cyclic tests in mm.

observation were thinned by jet-polishing in an electrolyte solution of 94 vol% acetic acid and 6% percloric acid. Finally, X-ray diffraction studies (XRD) were done to verify the absence of ε-martensite in the deformed stages during tensile or cyclic tests (not shown here). The measurements were carried out in a Siemens D-500 equipment using CuKα radiation with wavelength $\lambda = 0.1506$ nm.

The tensile and cyclic tests were carried out at room temperature in a MTS 250 kN testing machine. Tensile samples were machined from the initial sheet according to EN 10002-1 standard, with the tensile axis (TA) parallel to the rolling direction (RD) and a gauge length of 50 mm. For the cyclic tests, the geometry of the samples was designed to minimize buckling during reversal tests. Again, the tensile and compression axis were parallel to the rolling direction. The dimensions of the cyclic samples are illustrated in Fig. 1. In both tests, the strain rate was controlled at $8 \times 10^{-4}\ s^{-1}$.

In the case of the cyclic tests, an anti-buckling device inspired by the apparatus used by Boger et al. [5] was designed. Flat plates were used for buckling constraint, covering nearly all the free surface of the samples. The clamping system applied a constant force of 10 kN that corresponded to a stress of 5 MPa in both sides of the samples. A Teflon film with a thickness of 0.10 mm was inserted between the clamping system and the sample in order to reduce friction. The displacement was measured in the flank of the specimens using a Real time strain sensor (RTSS) video extensometer from Limess GmbH. The clamping and the measurement systems can be observed in Fig. 2. As described by Lee et al. [17] the constraint in the thickness direction during compression tests requires corrections to eliminate the effect of the friction and the biaxial effects. The friction coefficient was calculated by comparing the values of tensile tests without the clamping system

Fig. 2. Assembly of the anti-buckling device and the video-extensomenter for the cyclic test of sheet samples.

Please cite this article as: J.A. Benito, et al., Stress–strain response and microstructural evolution of a FeMnCAl TWIP steel during tension–compression tests, Materials Science & Engineering A (2016), http://dx.doi.org/10.1016/j.msea.2016.01.004

with the first tensile period of the cyclic tests in which the clamping system was installed. With regard to biaxial effects, the value of the effective stress in the thickness direction (− 5 MPa) is very small compared with the value of the initial yield stress of the TWIP steel used in this study, 480 MPa. Therefore, the variation of the effective stress was well below 0.5% and no additional correction was added [5].

3. Results

3.1. Tensile tests

The true stress–true strain curve for the TWIP Fe–17.5-0.7C–2Al steel is shown in Fig. 3. The values of yield strength (YS) and Ultimate Tensile strength (UTS) were 480 MPa and 1530 MPa, respectively. The total elongation was nearly 50%, which shows the good combination of high strength and ductility for this steel. The high strength of the present TWIP steel can also be related to the fine grain size (4 μm). Similar mechanical properties have been reported for other Fe–Mn–C TWIP steels of similar grain size [8,18]. Moreover, some contribution to strength is expected from carbon atoms dissolved in the austenite matrix, since the addition of 2% wt. of Al prevents cementite precipitation [12]. The analysis of the curve shows some micro-serrations from a strain of 0.3 up to the necking point. The addition of Al is also reported to decrease the number and the height of these micro-serrations, and in this case they appear at larger strain intervals and with lower step heights than in the case of Fe–Mn–C TWIP steels with no Al [12]. The plastic regime of the tensile curve was fitted to a Swift type hardening law and good correlation was observed, as also shown in Fig. 3. The stress hardening exponent n was as high as 0.69 ± 0.02, in consonance with other values found in literature [19].

The evolution of the strain hardening rate ($d\sigma/d\varepsilon$) of the present Fe–17.5Mn–0.7C–2Al steel is also plotted in Fig. 3. The general trend is very similar to that of Fe–19Mn–0.6C–2Al reported by Jin et al. [12] since no increase of strain hardening or even relatively constant values of hardening are observed during most of the deformation period. It is worth noting that the present steel has a higher strain-hardening rate than the one reported by Jin et al., the difference being around 300 MPa. This effect could be related to small differences in mechanical twinning rate or to the high activity of C atoms dissolved in the austenite matrix, since the present steel has a marked larger C content.

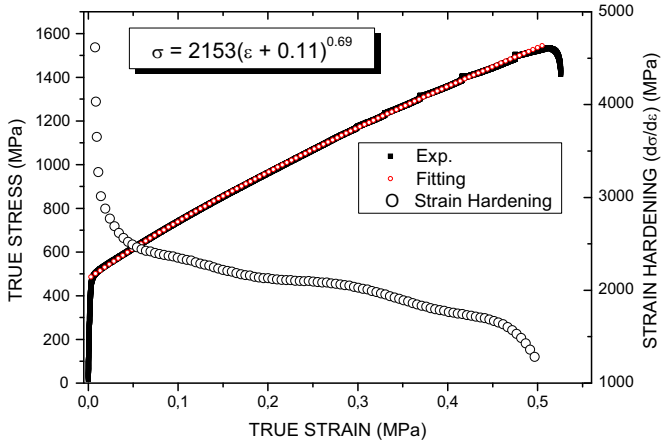

Fig. 3. Tensile stress–strain curve for the Fe–17Mn–0.7C–2Al TWIP steel together with the fitting curve using Swift's hardening law. The strain hardening evolution with strain is also displayed.

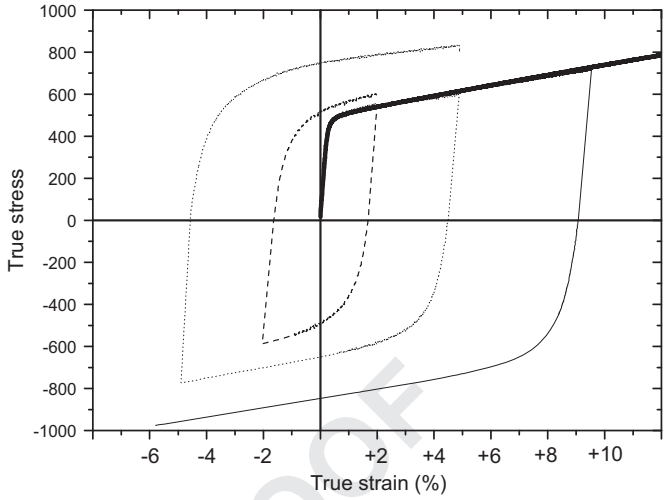

Fig. 4. Cyclic tests al different pre-strains together with the original tensile curve for the Fe–17Mn–0.7C–2Al TWIP steel.

3.2. Tension–compression tests

The tension–compression curves for cycles with strains of 2, 5 and 10% are displayed in Fig. 4. While for strains of 2% and 5% the cycles were completed satisfactorily, for a strain of 10% samples showed buckling in the unsupported gap when the compression step was close to finishing. Although the cycle with a strain of 10% was not fully characterized then, the compressive strain achieved was considered to be enough to reveal the Bauschinger effect and permanent softening at a pre-strain of 10%.

Regarding cycles with strains of 2% and 5%, cyclic hardening was observed and the increase of the stress at the end of the cycle was directly related to the strain of the cycle (60 MPa for a strain of 2% and 220 MPa for a strain of 5%). This behavior is in accordance with other studies in which the low-cycle fatigue of TWIP steels was investigated [6].

The evolution of the forward stress (σ_{for}) and reverse stresses (σ_{rev}) for each cycle is displayed in Fig. 5. For a better comparison, the reverse stage has been moved to the upper part by rotating 180°. As described elsewhere and pointed out for some TWIP steel compositions [7,20], in the reverse stage an early re-yielding can be observed at any forward strain applied, which is commonly referred to as Bauschinger effect (BE). All the curves in the reverse

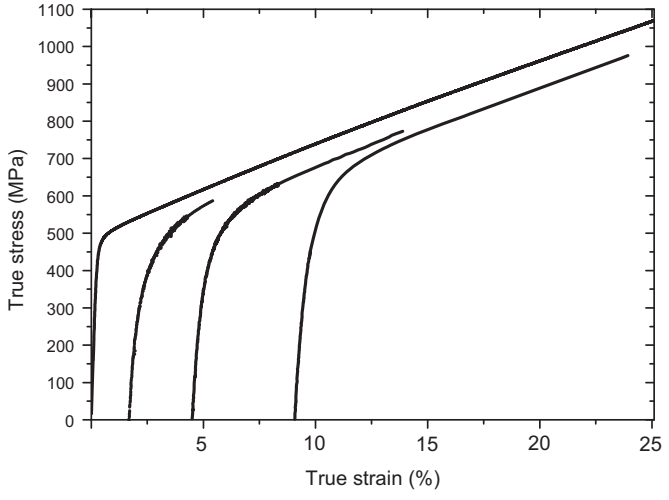

Fig. 5. Forward and reverse curves for the three pre-strains tested. Reverse curves are plotting with positive stress values for better comparison.

Please cite this article as: J.A. Benito, et al., Stress–strain response and microstructural evolution of a FeMnCAl TWIP steel during tension–compression tests, Materials Science & Engineering A (2016), http://dx.doi.org/10.1016/j.msea.2016.01.004

stage end up practically parallel to the forward curve after a "transient strain hardening" period, but they do not reach the values of the forward stress. Therefore, a "permanent softening" is observed in all cases. The difference between forward and reverse stress is related to internal polarized stresses commonly named back stress (σ_b) [8,10]. Back stress can be calculated by the Eq. (1):

$$\sigma_b = \frac{\sigma_{for} - \sigma_{rev}}{2} \quad (1)$$

Where σ_{for} is the stress at the end of the forward part of the cycle and σ_{rev} is associated to the yield stress after load reversal. In turn, σ_{rev} can be taken as the point of deviation from elasticity [20], or it can be determined by the 0.2% offset method [8,17] or from the point in which the forward and reverse curves become parallel after enough reverse strain [7]. In the case in which σ_{rev} is measured by the 0.2% offset method or by the deviation from elasticity, the back stress would be more related to the Bauschinger effect (BE). In the case in which σ_{rev} is determined at a strain in which the reverse and forward curves become parallel, the back stress would be related to permanent softening. It is interesting to define the strain at which back stress is measured since the values obtained by the 0.2% offset method are usually 2–3 times higher than those obtained from permanent softening. The difference seems to be independent from the type of steel and the type of test, whether shear or tension–compression. Here, for the sake of comparison, the back stress has been analyzed according to the 0.2% offset and permanent softening methods. The results are shown in Fig. 6. Together with the values for the present Fe–17.5Mn–0.7C–2Al steel, the results reported for other alloys are also included; namely, Fe–22Mn–0.6 C [7,8] obtained by reverse shear tests, Fe–24Mn–3Al–2Si–1Ni–0.06 C [20], a DP-steel [17], and a 316L stainless steel [21] determined by tension–compression tests. Tension–compression and shear tests are common experimental methods for observing the Bauschinger effect on sheet specimens [4,5]. The shear test enables to work at large strains and does not require corrections due to friction and biaxial stresses produced by the anti-buckling system, as is the case of tension–compression test [22]. Recently, different Advanced High Strength Steels including a TWIP steel were tested with both methods and the coefficients extracted from both test procedures were introduced into a hardening model [23]. The predicted flow curves in both cases were in reasonably good agreement, which suggests that the comparison between the data obtained from tension–compression and shear test makes sense. Therefore, the current research considers that no significant differences exist in the twinning activity of TWIP steels in both loading modes and that the mechanisms involved in the asymmetry of flow stress after load reversal are no significantly affected.

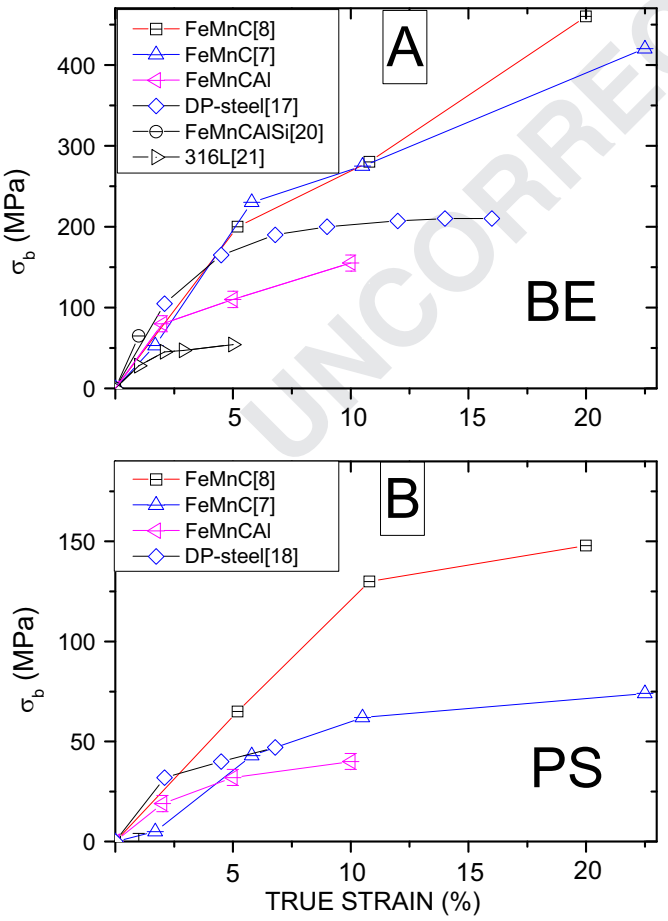

Fig. 6. Evolution of back stress with strain in reverse tests. (A) Bauschinger effect (BE): Values extracted with the 0.2% offset method. (B) Permanent Softening (PS): Values obtained from the point in which forward and reverse curves become parallel.

As already pointed out, the back stresses calculated with the 0.2% offset method were 2–3 times higher than the ones determined when the reverse curve is parallel to the forward curve. The difference seems to be independent from the type of steel and the kind of equipment used, shear or tension–compression test.

3.3. Back stress from the 0.2% offset method

As already stated, the back stress obtained with the 0.2% offset method focuses more on early re-yielding or BE. In Fig. 6a it can be observed that the BE increases rapidly in all cases as the forward strain is increased. At a strain of 2%, the increasing rate of the BE seems to be quite similar for all analyzed steels, independently of the composition, grain size and type of procedure used. From a strain of 5% forwards, although the BE maintains its growing behavior in all cases, some differences can be observed in the different steels. In the case of the DP-steel tested under tension–compression conditions the rate of increase tends to diminish as the strain increases, and from a strain of 10% the BE remains constant. For the 316 L austenitic stainless steel there is also a clear decrease in the rate of increase, and it seems that the behavior at larger strains could be similar to DP-steel. In the case of TWIP steels, although there is a drop in the rate of increase with respect to the rate at low strains, the BE keeps growing as the deformation increases. Nevertheless, the total amount of the BE is different depending on the type of TWIP steel analyzed. Thus, for the two FeMnC TWIP steels, a large increase is observed and the BE values are above 250 MPa at a strain of 10%, whereas for the present FeMnCAl TWIP steel the increment is smaller and at a strain of 10% the BE is around 150 MPa.

It is interesting to note that for FeMnC steels a constant increase of the BE is observed at larger strains up to 20–25%, and this trend coincides well with another study of a Fe–22Mn–0.6C with results very close to the present ones [24]. Although there is no data for FeMnCAl steel at these large strains, from the observation of the evolution of the BE with strain in Fig. 6a it is reasonable to think that the growing trend also appears for this steel at large strains, but with lower values than for FeMnC steels.

3.4. Back stress from the permanent softening method

The evolution of the back stress with pre-strain calculated by permanent softening is shown in Fig. 6b. The back stress for the present Fe–17.5Mn–0.7C–2Al steel behaves the same way as the others steels studied, i.e. an increase during the first period of plastic strain and stabilization as the deformation proceeds. For

Please cite this article as: J.A. Benito, et al., Stress–strain response and microstructural evolution of a FeMnCAl TWIP steel during tension–compression tests, Materials Science & Engineering A (2016), http://dx.doi.org/10.1016/j.msea.2016.01.004

Table 2
Calculations of back stress by the permanent softening method. The contribution of σ_b to hardening was calculated by $\sigma_b/(\sigma_{for}-\sigma_0)$. $\sigma_0=390\pm2$ MPa

Pre-strain	ε_{rev}	ε_{for}	$\varepsilon_{rev}/\varepsilon_{for}$	σ_{for} (MPa)	σ_{rev} (MPa)	σ_b (MPa)	Contribution to hardening (%)
0.02	0.032	0.02	1.6	623 ± 2	585 ± 5	19 ± 4	8 ± 2
0.05	0.045	0.05	0.9	725 ± 2	660 ± 5	32 ± 4	10 ± 2
0.10	0.052	0.10	0.52	860 ± 2	780 ± 5	40 ± 4	9 ± 2

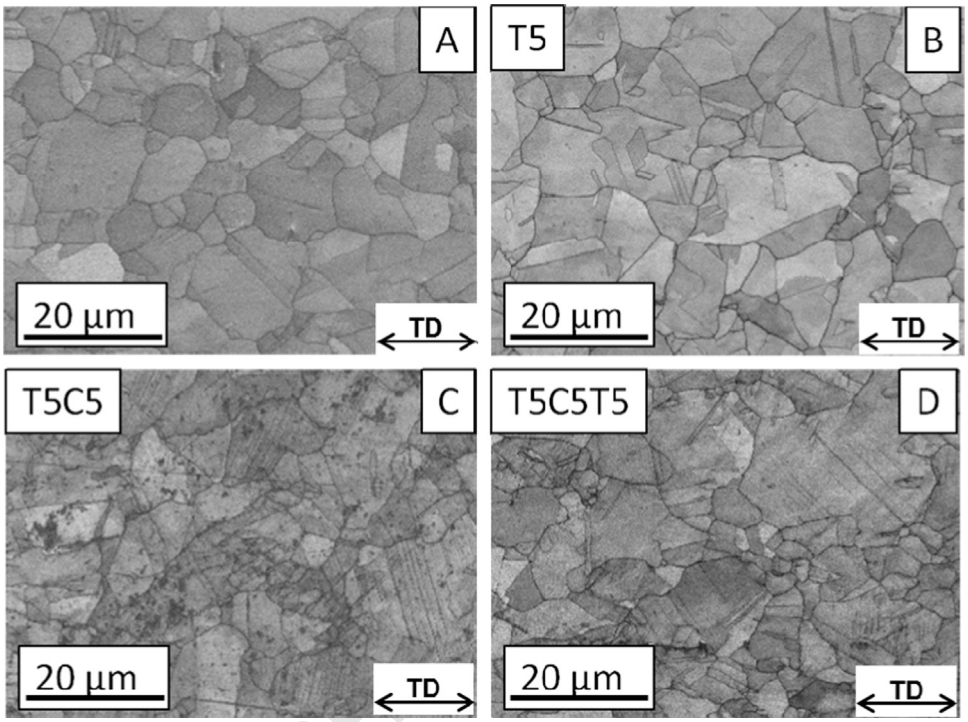

Fig. 7. Evolution of the microstructure of Fe–17Mn–0.7C–2Al TWIP steel during the cyclic test at 5% pre-strain. Image Quality maps obtained by EBSD. (A) Initial material; (B) First tensile stage at 5% strain (T5); (C) Compressive stage at −5% strain (T5C5); (D) Second tensile stage at 5% strain (T5C5T5). TD: Tensile direction.

this Fe–17.5Mn–0.7C–2Al alloy the back stress is 19 ± 4 MPa at a strain of 2%, 32 ± 4 MPa at 5% and the maximum value obtained is 40 MPa $\pm$ 4 at a strain of 10%. Comparing with the DP-steel or with the Fe–22Mn–0.6C TWIP steel with coarse grain, the values are close but slightly lower. However, with respect to the Fe–22Mn–0.6C steel with a fine grain size of 3 μm [8] the back stress of the present steel is clearly lower, the difference being, at a strain of 10%, around 100 MPa.

As pointed out by Gutierrez et al. [7] the experimental values of σ_b obtained from the permanent softening method and X-ray diffraction techniques are in better agreement, and therefore more consistent, when the strain needed to become parallel (ε_{rev}) in the reverse curve is of only around 50% of the previous forward strain (ε_{for}). In the case of reverse shear tests for the Fe–22Mn–0.6 C TWIP steel, the ratio $\varepsilon_{rev}/\varepsilon_{for}$ seems to be clearly below 1 in any case [7,8]. In order to verify if the present calculations fulfill this condition, the results of the calculations between forward and reverse stages in the tension–compression tests for the present TWIP steel are listed in Table 2. The ratio between ε_{rev} and ε_{for} needed to get parallel curves is calculated for the three pre-strain cases and it decreases as the amount of pre-strain increases, ranging from 1.6 for a pre-strain of 2% to 0.52 for a pre-strain of 10%. This behavior is similar to the case of the DP-steel, in which the ratio $\varepsilon_{rev}/\varepsilon_{for}$ is nearly 2 for a strain of 2.1%, decreasing to 0.7 at a pre-strain of 6.8%. In both cases, tension–compression tests were used. The analysis of the evolution of $\varepsilon_{rev}/\varepsilon_{for}$ with pre-strain shows that only in the case of a strain of 2% the back stress from permanent softening could be affected and the values obtained inaccurate. Consequently, this effect could explain the difference between the back stress of the Fe–17.5Mn–0.7C–2Al steel at a strain of 2% (19 MPa) and the low value for the Fe–22Mn–0.6C alloy, 5 MPa at the most. For the rest of the pre-strains conditions, the obtained back stress values with the permanent softening method would be well estimated.

Finally it has to be mentioned that for the Al-added TWIP steel, the calculated contribution of back stress to the total work hardening is less than the calculated value reported for the other TWIP steels mentioned. For the Fe–17.5Mn–0.7C–2Al steel this contribution is 8% at a pre-strain of 2% and increases only to 10% with pre-strains of 5% and 10%, whereas for Fe–22Mn–0.6 C steels it was slightly below 20% [7] and around 40% [8].

3.5. Evolution of dislocation and twin structure during a cycle with a pre-strain of 5%

To analyze the evolution of the microstructure during cycles with a strain of 5%, one sample was stopped at the end of the first tensile stage at a strain of 5% (sample named T5), another one was stopped at the end of the compressive stage at a strain of −5% (sample named T5C5), and one sample was studied at the end of the complete cycle (sample named T5C5T5). The evolution of the microstructure was first observed by EBSD, but since the twin thickness was smaller than 100 nm (as will be reported in the TEM analysis), which is in the order of magnitude of the step size used, the presence of mechanical twins by automated EBSD analysis was hardly noticeable. However, their presence was easily observed in

Please cite this article as: J.A. Benito, et al., Stress–strain response and microstructural evolution of a FeMnCAl TWIP steel during tension–compression tests, Materials Science & Engineering A (2016), http://dx.doi.org/10.1016/j.msea.2016.01.004

the Kikuchi Pattern quality (KPQ) map. For this reason, the KPQ maps in the longitudinal plane for the initial material and the stages T5, T5C5 and T5C5T5 are presented in Fig. 7. In all the images, the tensile direction (TD) coincides with the original longitudinal hot rolling direction. In the as-received material (Fig. 7a) the aspect ratio of the grain taking into account the annealing twins is 2.18 ± 0.10, as a consequence of the rolling process. Some annealing twins can be observed distributed homogeneously over the grains.

After the first tensile stage, the aspect ratio of the grain increased to 2.39 ± 0.10 as a result of tensile deformation, but in the KPQ for T5 sample (Fig. 7b) mechanical twins were hardly noticeable. The small presence of mechanical twins at low strains has been reported before for different types of TWIP steel as, for instance, in the Fe–22Mn–0–6C steel with a tensile strain of 5% [25,26]. Moreover, as already stated, the addition of Al is referred to decrease the rate of mechanical twinning in Fe–22Mn–0.6C [12] so in the present Fe–17.5Mn–0.7C–2Al steel or in the Fe–22Mn–0.6C–1.5Al alloy [15] this slight presence of mechanical twins can be justified. At increasing strains, see Fig. 7c and d, mechanical twins are readily apparent. Regarding the dislocation structure observed by TEM (Fig. 8a), no planar arrangement of dislocations is

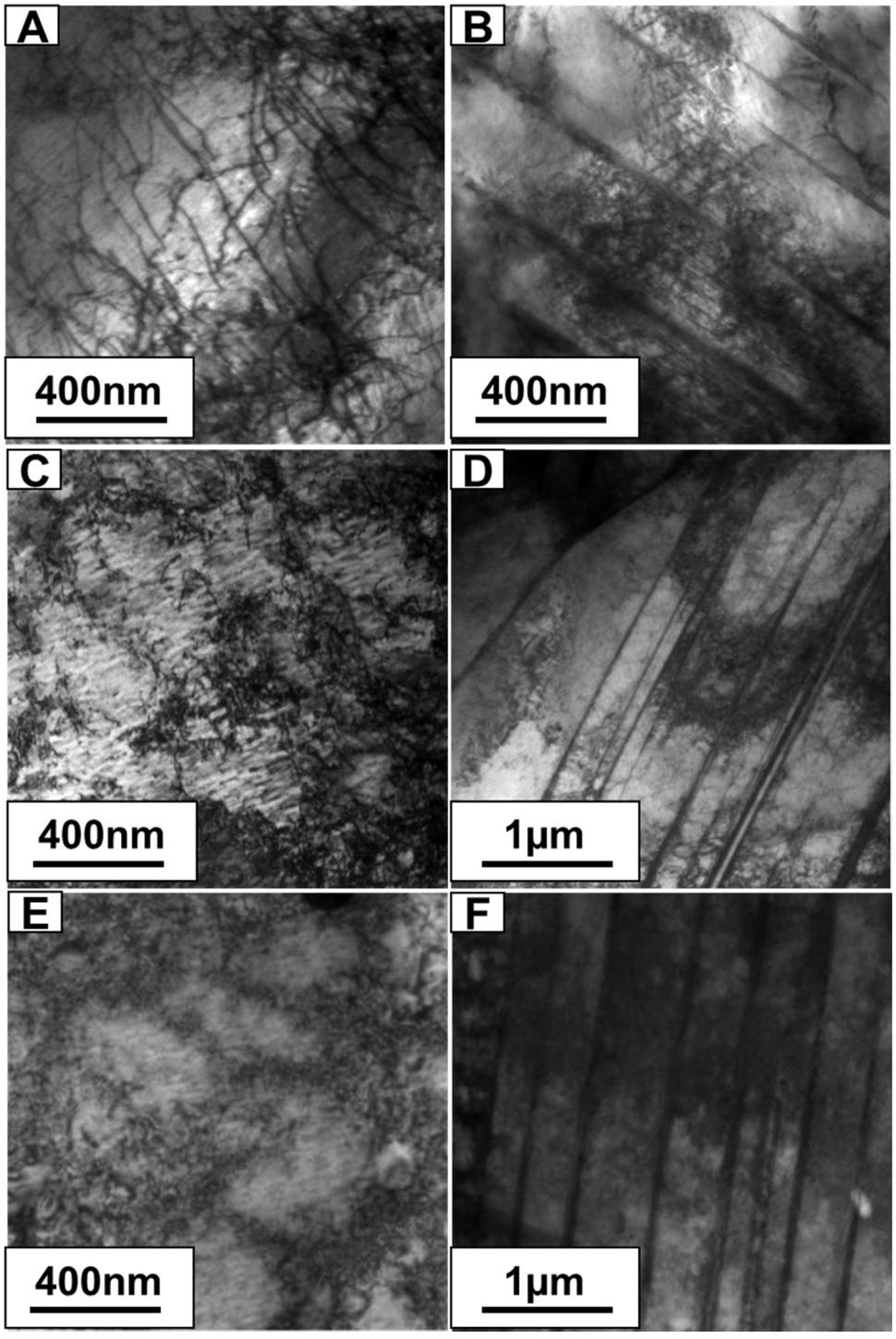

Fig. 8. TEM micrographs showing the evolution of dislocation structure and mechanical twins for the cyclic test at 5% pre-strain. (A and B) After first tensile stage at 5% strain (T5); (C and D) After compressive stage at −5% strain (T5C5); (E and F) After the second tensile stage at 5% strain.

Please cite this article as: J.A. Benito, et al., Stress–strain response and microstructural evolution of a FeMnCAl TWIP steel during tension–compression tests, Materials Science & Engineering A (2016), http://dx.doi.org/10.1016/j.msea.2016.01.004

noticed, although long dislocation lines can be observed in many grains. However, these long segments of dislocations are prone to be entangled so the structure seems to be closer to a dislocation forest. This structure is more similar to the one described for fine-grained Fe–22Mn–0.6C steels with an average grain size around 3 μm [26,27] than to the one of the Fe–22Mn–0.6C steel with an average grain size of 50 μm [25], since no dislocation cells were detected after a tensile strain of 5%. Regarding the mechanical twins, following the evolution of the calculated twinning fraction for a similar composition to the present Fe–17.5Mn–0.7C–2Al steel, at a tensile strain of 5% a very small twinning fraction would be expected [13]. Fig. 8b shows one of the scant bundles of twins and it is worth noting the higher dislocation density in the space between twins compared to the untwinned grain in Fig. 8a. The average twin thickness calculated from the small number of twinned grains is 40 ± 15 nm, whereas the average twin spacing is about 180 ± 50 nm.

The microstructure in Fig. 7c for the sample after the compressive stage (T5C5) shows how the grains have been now compressed due to reverse straining in the former TD and consequently the aspect ratio decreased to 2.09 ± 0.10. In fact, this sample has undergone a compressive strain very close to 10%, and the accumulate strain is around 15%. Therefore, it is understandable that many grains show thick bundles of mechanical twins after the compressive stage. The analysis of dislocation structure by TEM in Fig. 8c shows that many dislocation cells have appeared with very low dislocation density inside of them. The average diameter of these cells was 450 ± 100 nm. The analysis of the twins by TEM (Fig. 8d) showed that generally only one twin system is active and very rarely a secondary system is observed. The diminution of active systems in Al-added TWIP or Hadfield steels is reported in the literature [12,15,28]. In this case, the twin thickness, 60 ± 15 nm, was larger than in the first tensile stage. The twin spacing was also calculated and it was 220 ± 60 nm.

The microstructure after the second tensile stage (T5C5T5) is displayed in Fig. 7d. The aspect ratio of the grains increases again up to 2.25 ± 0.10, which indicates the new elongation of grains following TD. The tensile strain in this stage was 10%, so the total accumulated strain at the end of the cycle for the T5C5T5 sample was 25%. The analysis of the microstructure shows a great number of twinned grains but without a clear increase in dense bundles of twins, as compared to T5C5 condition. Moreover, secondary twinning is a little more active than in the case of T5C5. With regard to dislocation activity, a refinement of cell structures is observed, since they have an average value of 300 ± 100 nm, smaller than in the case of T5C5 (Fig. 8e). This process has been well documented for other TWIP steels [6,26,27]. The twin thickness shows a very wide distribution ranging from 20 to 150 nm. Grains with bundles of twins with average thickness around 120 nm are easy to find (Fig. 8f), but some small grains with narrow twins with a thickness of 20–30 nm have also been observed. Twin spacing also depends on the type of bundle, being 300 nm for the thicker twins and around 100 nm for the narrow ones.

3.6. Texture evolution during a cycle with a pre-strain of 5%

Fig. 9 shows the evolution of texture represented by the Orientation Distribution Function (ODF) at $\varphi_2 = 45°$ section in the Euler space and the inverse pole figure (IPF) along the tensile direction (TD) for the initial material and the final steps of the cycle with a strain of 5%. The initial texture of the as-received material is displayed in Fig. 9a; shows the presence of Brass $\{110\}<112>$ and Goss $\{110\}<001>$ texture components, although the latter with a weak signal. These orientations are commonly associated with hot rolled fcc metals [29]. On the other hand, the presence of cube component $\{001\}<100>$ must be noted, which may be related to the compressive behavior in the center of the sheet during hot rolling [30]. These components are reflected in the IPF, since poles $<111>$ and $<001>$ are the strongest components.

After the first tensile stage up to a strain of 5% (T5), there is an increase of the signal for rotated Brass $\{110\}<111>$ and Goss orientations, both of them typical texture components during tensile deformation of TWIP steels [12,31]. At the same time, the cube texture component is also clearly visible. The presence of these orientations is reflected in the increase of the intensity in poles $<111>$ and $<100>$ of the IPF, which has also been described for other TWIP steels deformed by tensile tests [13,25].

When the samples are deformed in compression to a strain of −5%, some changes are observed in the $\varphi_2 = 45°$ ODF section in Fig.9c. There is a clear increase of cube component $\{001\}<100>$, with a maximum orientation density of 3.15 and the appearance of rotated-Cube component $\{001\}<101>$, with values of

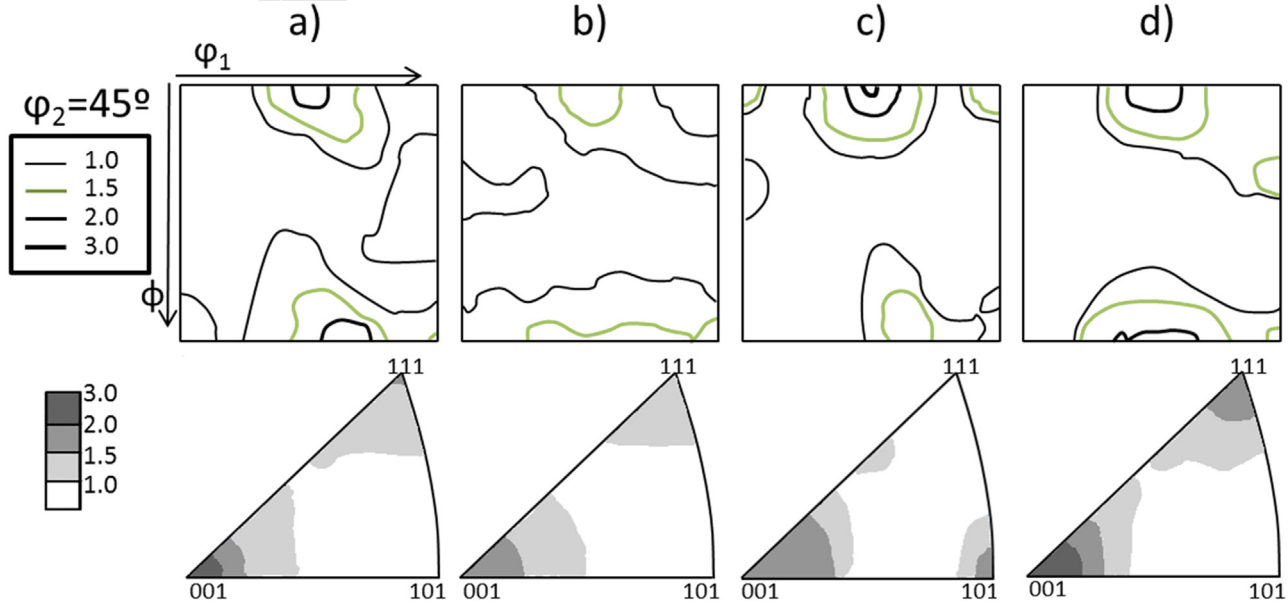

Fig. 9. ODF in $\varphi_2 = 45°$ sections and IPF for the as-received material and after different strain levels. (a) as-received material; (b) after 5% tensile strain (T5) (c) after compressive stage to −5% strain (T5C5) and (d) after second tensile stage at 5% strain (T5C5T5).

orientation density around 1.5. The growing cube and rotated-Cube components during compression were not reported as predominant orientations in high-manganese steels [32]. However, there are some coincidences in the evolution of grain orientations. First, and according to the evaluation of Schmid factors for twinning and dislocation slip in compression [14,33] twinning is favored in $<001>$ oriented grains. This fact was observed in the work of Meng et al. and the same result has been observed in the present Fe–17.5Mn–0.7C–2Al steel since most of the grains that contain mechanical twins in the KPM in Fig. 8c are oriented in direction $<001>$. At the same time, looking at the IPF in Fig. 9c, there is an increase of grains in direction $<101>$. This increase is related to the grain rotation due to slip [32] and could explain the increase of some components such as rotated-cube $\{001\}<101>$ or even rotated-Cu $\{112\}<101>$. As shown by the present TEM studies, during the compression stage both the twinning and dislocation slip have proceed normally and the evolution of grain orientations can be considered consistent with the compressive behavior of TWIP steels.

After the second tensile stage at a strain of +5%, the resulting texture in the $\varphi_2=45°$ ODF section of Fig. 9d shows the strengthening of the components related to tensile deformation in TWIP steels [13,31] indicated by an increase in the orientation density around Brass and rotated-Brass components. Although the predominant component at high strains is rotated-Brass, at low strains the maximum densities are clearly not close to the exact Euler angles [13]. Additionally, there is a slight increase of Goss component and an especially clear development of Cu component $\{112\}<111>$. The aspect of the IPF in this T5C5T5 stage in Fig. 9d shows a clear development of orientations in poles $<001>$ and $<111>$ that coincide with the usual description for the tensile deformation of TWIP FeMnC and FeMnCAl steels [13,25]. However, in this case fiber $<111>$ appears with an intensity lower than $<001>$, as opposed to what is usually observed in TWIP steels [13,25,31]. There may be several reasons for this behavior: on the one hand, a 10% tensile deformation can be considered low for developing a well-defined texture comparing with other studies in which the strain was at least over 20% [13,25,31], particularly in this case, in which in addition, there are changes in the deformation path. On the other hand, although cube component $\{001\}<100>$ has been observed in the tensile texture of FeMnC TWIP steels [31], its intensity in the present case is higher than expected and it can be related to its strong presence in the initial texture (Fig. 9a).

4. Discussion

Following the same procedure used in the section above, it is necessary to divide the discussion on back stress in two parts: Firstly, concerning early re-yielding during reverse stress, i.e. what here is defined as the Bauschinger effect (BE), and secondly, taking into consideration the difference between forward and reverse stresses when both curves become parallel when permanent softening (PS) is noticed.

4.1. Bauschinger effect

Looking at the evolution of the BE with pre-strain in Fig. 6a, it is clear that at low strains, the BE is quite similar for all the materials studied, including a Fe–24Mn–3Al–2Si–0.06C TWIP steel in which only the BE at a pre-strain of 1% using the 0.2% offset method has been determined [20]. At a pre-strain of 2%, the most common feature is that the BE increases rapidly for all the materials studied. At these low strains, a very limited effect of twinning is expected in TWIP steels due to the small number of twinned grains detected in the present steel and others TWIP steels [25,27,34]. Under these conditions, as pointed out by Saleh et al. [20], there must be other contributions to the back stress of TWIP steels at these low strains. In this point is interesting to revisit some results of 316L and 317 austenitic steels that do not twin [21,35]. It has been reported that in the case of these steels planar slip is favored during the early stages of deformation. The generated dislocations move under the applied stress causing many pile-ups and stacking faults [36]. Under load reversal conditions some of the dislocations can move back causing a source of back stress [21,35,36] for 316L austenitic steel, as shown in Fig. 6b. It is interesting to note that stacking faults also interact with dislocations and this have been considered as another source of back stresses [20,35].

When the pre-strain attains to 5%, the differences between the various materials start to increase. The differences in the amount and rate of increase of the BE with strain must be related to the strengthening mechanisms acting in every particular case.

Firstly, there is a Dual-Phase steel in which the microstructure consists of hard martensite (12%) and a soft ferrite matrix [17]. Although DP-steels have shown fairly good strength and ductility, the strengthening mechanism is different from that of TWIP steels. In the absence of twinning and precipitates in the ferrite matrix, the slip of dislocations and their storage by intersections is the main hardening mechanism, helped by the presence of hard martensite plates. In bcc metals, the dislocations generated in the early stages of deformation tend to be stored in high density dislocation walls forming cell boundaries [37]. After a certain amount of monotonic deformation, it is accepted that these dislocation structures evolve towards steady-state configurations. Once the cell structure is formed, the polarization reaches a maximum and further strain can refine the cell diameters slightly but, in essence, the back stresses generated remain constant. This depletion in the source of back stress with strain in DP-steels is shown clearly in Fig. 6a since from a strain of 10% the BE values remain constant, although some isotropic hardening is still present at these strains levels [17].

A similar situation can be observed in the case of 316L austenitic steel. After the first stage of deformation ($\approx 1.5\%$), a transition from planar slip to wavy slip has been described; it has also been observed that the number of grains presenting different dislocation interactions due to cross-slip increases [36]. Therefore, as in the case of DP-steels, at larger strains the hardening tends to be isotropic, which causes a clear diminution of the back stress increase rate. This effect can be observed in Fig. 6a since from a strain of 2–5% the back stress for 316L steel shows a very small increase.

Compared to DP and 316L steels, TWIP steels show no signs of reduction in the rate of increase of the BE at the pre-strains analyzed in Fig. 6a. This continuous increase of the BE has been related to the interaction of the twin lamellae with dislocations. This mechanism has been defined as a strong source of back stresses in TWIP steels and acts over larger strain periods [7,8,10,25,27].

In particular, models for the increment of back-stress [8,10], make it possible to link the kinematic hardening created by the accumulation of dislocations in the matrix at twin boundaries with twin volume fraction and thickness. Accordingly, an equation for the back stress (σ_b) used by Bouaziz et al. and proposed by [38] is used here:

$$\sigma_b = M\frac{\mu \cdot b}{L}n \tag{2}$$

where M is the average Taylor factor, μ is the shear modulus, b is the burgers vector, n the number of dislocations stopped at the boundary and L the mean intercept length. In turn, the dependence of L with strain can be expressed by the following relation:

Please cite this article as: J.A. Benito, et al., Stress–strain response and microstructural evolution of a FeMnCAl TWIP steel during tension–compression tests, Materials Science & Engineering A (2016), http://dx.doi.org/10.1016/j.msea.2016.01.004

$$L = 2t\left(\frac{1-f_v}{f_v}\right) \quad (3)$$

where t is the twin thickness and f_v is the twin volume fraction.

The continuous increase of the BE for TWIP steels up to 20% strain observed in Fig. 6a can be explained by Eqs.(2) and (3). It has been shown that twinning in TWIP steels can be active for larger strains up to 0.50 [14,25]. Therefore, f_v is expected to grow continuously during all this period giving smaller values of L. Moreover, as TWIP steels are deformed, there is an increase of the dislocation density that enhances the interactions between dislocations and twin boundaries, rendering a continuous increase of n in Eq. (2). Both contributions promote an increase in σ_b. This increase in dislocation activity around twin boundaries can be observed in the TEM micrographs for the material strained to 5% (T5). In the grains with no twinning activity (Fig. 8a), long dislocations lines are observed, whereas in the grains with twin bundles (Fig. 8b) the dislocation lines are shorter and the intersections more frequent.

Firstly, the validity of this mechanism in TWIP steels at low strains due to the low twinning activity must be discussed. There is some variability between different works in the literature about the twinning activity at a pre-strain of 5% in TWIP steels. In some cases, it has been found that the number of grains with mechanical twins is moderate, with a $f_v \approx 0.05$ [31]. In addition, the presence of twinning activity has a clear influence in the work hardening rate since it starts to increase at these low strains [31]. In other cases, the f_v at this pre-strain is smaller, and the twinned grains are more difficult to be seen [12,15,25,34]. Consequently, the typical increase of the work hardening rate due to twinning activity is not observed, although in some cases the hardening rate is already almost constant [25]. In this situation, at a pre-strain of 5% it is reasonable to think that although twinning has a growing role in the overall mechanical response of TWIP steels and its influence in the development of back stress is large, other sources of back stress could still play a significant role.

As mentioned above, stacking faults can act as a source of back stress. Here it is interesting to note that at low strains, the presence of overlapped stacking faults has been described in FeMnC steels and other fcc metals [39]. In addition, they have been considered as a previous step in twin formation [39–41]. This suggests that a significant presence of stacking faults is feasible and consequently some contribution from them to the overall back stress on TWIP steels at a pre-strain of 5% could be expected.

In the case of a pre-strain of 10%, it can be considered that the effect of twinning activity on the mechanical behavior of TWIP steels is even more important. This strain marks approximately the beginning of the high work hardening stage and the fraction of primary twinned grains is between 20 and 30% [12,15,25,34]. In addition, in FeMnC TWIP steels there is a clear increase of the secondary twinned grains [15,34]. In this scenario, twinning activity affects the overall behavior of the material and the interaction of twin lamellae with dislocations can be considered as the main source of back stress in TWIP steels. Therefore, it might be concluded that the mechanism for the increment of the back stress proposed above could be applied from this strain for the TWIP steels studied here.

Secondly, although this mechanism can be applied to all TWIP steels in Fig. 6a, there are marked differences in the total amount of the BE between the Fe–22Mn–0.6C steels and the Fe–17.5Mn–0.7C–2Al steel presented here. At 5% and 10% strain, the BE of Fe–22Mn–0.6C steels is nearly twice the value of the Fe–17.5Mn–0.7C–2Al steel. Here it is important to point out that the forward stress (σ_{for}) at pre-strains of 5% and 10% are quite similar for the three steels, around 600 MPa and 700 MPa respectively. It means that the contribution of back stress to the total stress in the case of Fe–22Mn–0.6C steels doubles the one of the Fe–17.5Mn–0.7C–2Al steel. While in Fe–22Mn–0.6C steels the contribution of BE is slightly less than half the total stress [7,8,10], for the present TWIP steel this value is around 20%. This effect can be attributed to the role played by aluminum in TWIP steels.

As pointed out in the work by Jin et al. [12], the presence of aluminum hinders the precipitation of (Mn,Fe)C in the Fe–18Mn–0.6C steel and decreases the activity of C atoms in the austenite matrix, weakening the pinning force of these atoms on mobile dislocations. The latter effect leads to a reduction in the Dynamic Strain Aging (DSA) phenomenon [42], which is reflected in the delay and the diminution in the step height of the serrations in the tensile curve of Al-added TWIP steels [13]. Moreover, the addition of aluminum to FeMnC TWIP steels increases the Stacking Fault Energy (SFE), which promotes a decrease in the activity of mechanical twinning and a certain increase of the dynamic recovery effect [43]. The extent of the decrease in primary mechanical twinning varies depending on the authors, but in the case of secondary mechanical twinning a large reduction has been reported [12,15,28]. This decrease in the activity of mechanical twinning and the increase in dynamic recovery means that the strain hardening of FeMnCAl TWIP steels is clearly lower than the one for FeMnC TWIP steels of similar composition [14,15,43] and similar grain size [27].

This decrease of twinning activity for Al-added TWIP steels can then be related to the lower values of the BE as derived from Eqs. (2) and (3). According to several works [12,14,15], the value of f_v for the present Fe–17.5Mn–0.7C–2Al steel would be lower than for the Fe–22Mn–0.6C steel. Concerning twin thickness t, the average value observed in the present samples at a tensile strain of 5% (T5) was 40 ± 15 nm, which can be considered slightly low and mainly influenced by the fine grain size [25]. In FeMnCAl TWIP steels tested at similar strain rate and with a grain size of 40 μm, a wide range of average twin thickness has been reported, from 15 nm to 120 nm [15,16]. For the Fe–22Mn–0.6C TWIP steels tested at similar strain rates, lower values of t, between 10 and 40 nm, were reported when studying fine-grained materials [26], whereas the t average values were 17 ± 5 and 16 ± 8 nm when considering coarse grained (40 μm) materials [15,16]. These results might suggest that the twin thickness in the present FeMnCAl steel can be larger than in the case of the fine-grained Fe–22Mn–0.6C steel studied by Bouaziz et al. [8] and similar to the coarse-grained Fe–22Mn–0.6C Steel studied by Gutierrez et al. [7], since they estimated twin thicknesses between 30 and 60 nm. Therefore, it can be concluded that in Eq. (3) the mean intercept length L for the present FeMnCAl TWIP steel should be larger than for the FeMnC TWIP steels.

In the Eq. (2), apart from L, the term n accounts for the dislocations stopped at the grain and twin boundaries. As shown in Fig. 8a, there is a big difference in the dislocation density between twinned and untwinned grains, since in the former ones there are a great number of dislocations which are trapped in the twin spacing. At the strains levels studied here, little twinning activity is generally reported, although it is not null, and in some cases, at low strains (i.e., 2%) a direct effect of twinning has been related to an increase of the strain hardening [15,25,26]. Again, as exposed before, FeMnCAl TWIP steels tend to generate less number of twinned grains than FeMnC TWIP steels [12,15,28], so it is expected that n should be lower for the present FeMnCAl steel than for the FeMnC steels.

Therefore, Eq. (2) can offer a reasonable explanation for the lower values of the BE observed in the present Fe–17.5Mn–0.6C–1.5Al steel, as compared with the Fe–22Mn–0.6C steel, mainly based in the slower rate of mechanical twins in the Al-added TWIP steels.

Please cite this article as: J.A. Benito, et al., Stress–strain response and microstructural evolution of a FeMnCAl TWIP steel during tension–compression tests, Materials Science & Engineering A (2016), http://dx.doi.org/10.1016/j.msea.2016.01.004

4.2. Permanent softening

It must be borne in mind that the back stress is measured by Eq. (1), but at strains in which the forward and reverse curves are nearly parallel; this means that the back stress is measured after the "transient hardening" period during which most of the dislocations initially piled-up in twin boundaries and grain boundaries have moved backward. Moreover, as the strain increases in the reverse direction the combination of dislocation and twinning activity hardens the material.

Before analyzing the differences between the different materials, the fact that very similar strain hardening behavior is observed during the tensile and compression periods in Fig. 5, should be mentioned. It should be noted that the same behavior was observed in other cyclic tests on TWIP steel [7,8]. The study of the microstructure after the compression period in the 5% cyclic test (T5C5 samples) shows that there is an evolution in dislocation and twinning activity. On the one hand, the dislocations tend to create a cell structure (Fig. 8c), which has been also observed in Fe–22Mn–0.6C steels [6,25]. On the other hand, as observed in Fig. 7c there is a clear increase of the amount of grains in which bundles of mechanical twins are observed. Although it has been shown that in cyclic tests with low strain amplitude (up to 1%) twinning has limited activity in the compression half of deformation cycles [6,20]; in the present case for the deformation cycle of 5% the strain in the compression half is 10%, which seems to be large enough to promote twinning activity. At the same time, the compression strain intervals studied here do not seem to be large enough to observe the decrease of twinning activity that is associated to the rotation of most of the twinned grains from orientations $<100>$ to $<110>$ as the compressive strain increases. This decrease in twinning activity would lead to a decrease in strain hardening [32]. Therefore, after "transient hardening" period, no microstructural changes that could lead to significant differences in the strain hardening between tensile and compressive periods have been found.

With regard to the back stress values obtained by permanent softening for the different type of steels, it seems that in general, increase stops at large strains. This was more or less expected for the DP-steel since the same situation was found in analyzing the BE, due to the dislocations slip and creation of dislocations cells. In the case of TWIP steels, the values for the present Al-added TWIP steel are slightly lower than the ones for the Fe–22Mn–0.6C steel with a large grain size [7,25]; both are more or less half of the fine grain size Fe–22Mn–0.6C steel [8]. It must be taken into account that the contribution of back stress to the total stress in the Al-added TWIP steel is around 10–12%, whereas for the large grain-sized FeMnC steel it is around 18% and near 40% for the low grain-sized FeMnC. The lower twinning activity in the Al-added TWIP steel could again explain, by using Eqs. (2) and (3), the relative low values of back stress for this steel with regards FeMnC TWIP steels.

In order to understand the reason for the permanent softening during reverse stage in the present FeMnCAl steel, one factor that could play a role would be the twin thickness t, since in the compressive stage this parameter appeared to be slightly higher than for the first tensile stage, 60 ± 15 nm and 40 ± 15 nm, respectively. At the same time, twin spacing has grown a little, i.e. from 180 ± 50 nm to 220 ± 60 nm. According to Eq. (3), the increase of t would lead to a larger L. In addition, this bigger twin spacing could be related to a smaller increase of the amount of dislocations stopped at twin boundaries, which would mean lower values of n. Therefore, the increase of twin thickness and twin spacing would be the two microstructural features that might explain the decrease of the flow stress during the compressive stage for the present Al-added TWIP steel.

5. Conclusions

The FeMnCAl TWIP steel studied shows a continuous increase of the back stress during reverse loading in the compression stage as the pre-strain is increased to 10%. This trend coincides with the behavior of some FeMnC TWIP steels reported in literature and is consistent with existing hardening models for TWIP steels. When the back stress is analyzed using the 0.2% offset method and related to the Bauschinger effect, the value of the back stress for the FeMnCAl TWIP steel and its contribution to the total hardening is half the one reported for FeMnC TWIP steels. This behavior can be related to the decrease of mechanical twinning activity in Al-added FeMnC TWIP steels, since it has been reported that the primary source of polarized internal stresses in these steels consists on the dislocations pinned in the matrix by twin boundaries.

When the back stress is analyzed by permanent softening measurements, the values are in all cases much smaller than in the case of the Bauschinger effect. The FeMnCAl steel shows again lower values than FeMnC steels, which can once more be related to the lower twinning activity of FeMnCAl steels.

For the present FeMnCAl steel the strain hardening in tensile and compressive stages is very similar. It has been found that the twin thickness and twin spacing appeared slightly larger in the compressive stage. Since the increase of both parameters is related to a diminution of the kinematic hardening, they could explain the differences between the tensile and compressive strengths after the transient hardening period for the FeMnCAl TWIP steel.

Acknowledgments

The authors would like to thank the Spanish Ministerio de Economia y Competitividad (project ref. MAT2014-59419-C3-1-R) and the Agència de Gestió d'Ajuts Universitaris i de Recerca de la Generalitat de Catalunya (project 2010 CONE3 42) for the economic support and Posco (South Korea) for supplying the steel studied.

References

[1] P.A. Eggertsen, K. Mattiason, Int. J. Mech. Sci. 51 (2009) 547–563.
[2] F. Yoshida, T. Uemori, Int. J. Mech. Sci. 45 (2003) 1687–1702.
[3] L. Geng, R.H. Wagoner, 2000. SAE paper No. 2000-01-0768. SAE, Inc.
[4] S. Bouvier, H. Haddadi, P. Levée, C. Teodosiu, J. Mater. Process. Technol. 172 (2006) 96.
[5] R.K. Boger, R.H. Wagoner, F. Barlat, M.G. Lee, K. Chung, Int. J. Plast. 21 (2005) 2319–2343.
[6] H.-G. Lambers, C.J. Rüsing, T. Niendorf, D. Geissler, J. Freudenberger, H.J. Maier, Int. J. Fatigue 40 (2012) 51–60.
[7] I. Gutierrez-Urrutia, J.A. Del valle, S. Zaefferer, D. Raabe, J. Mat. Sci. 45 (2010) 6604–6610.
[8] O. Bouaziz, S. Allain, C. Scott, Scr. Mater. 58 (2008) 484–487.
[9] I. Karaman, H. Sehitoglu, Y.I. Chumlyakov, H.J. Maier, I.V. Kireeva, Met. Mater. Trans. A 32 (2001) 695.
[10] J. Gil Sevillano, Scr. Mater. 60 (2009) 336–339.
[11] O. Bouaziz, S. Allain., C.P. Scott, P. Cugy, D. Barbier, Curr. Opin. Solid State Mater. Sci. 15 (2011) 141–168.
[12] J.-E. Jin, Y.-K. Lee, Acta Mater. 60 (2012) 1680–1688.
[13] B.C. De Cooman, J. Kim, S. Lee, Scr. Mater. 66 (2012) 986–991.
[14] Y.-K. Lee, Scr. Mater. 66 (2012) 1002–1006.
[15] H.K. Yang, Z.J. Zhang, Z.F. Zhang, Scr. Mater. 68 (2013) 992–995.
[16] H.K. Yang, Z.J. Zhang, F.Y. Dong, Q.Q. Duan, Z.F. Zhang, Mat. Sci. Eng. A607 (2014) 551–558.
[17] M.-G. Lee, D. Kim, C. Kim, M.L. Wenner, R.H. Wagoner, K. Chung, Int. J. Plast. 21 (2005) 883–914.
[18] J.-E. Jin, Y.-K. Lee., Mater. Sci. Eng. A 527 (2009) 157.
[19] H. Ahn, D. Yoo, M.H. Seo, S.-H. Park, K. Chung, Met. Mater. Int. 15 (2009) 637–647.
[20] A.A. Saleh, E.V. Pereloma, B. Clause, D.W. Brown, C.N. Tomé, A.A. Gazedr, Acta Mater. 61 (2013) 5247–5262.
[21] M. Choteau, P. Quaegebeur, S. Degallaix, Mech. Mater. 37 (2005) 1143–1152.
[22] T. Kubawara, Y. Morita, Y. Miyashita, S. Takahashi, Proc. Int. J. Plast. 233–236

(2007) 287–292.
[23] J.S. Choi, J.W. Lee, J.-H. Kim, F. Barlat., M.G. Lee, D. Kim., Int. J. Mech. Sci. 98 (2015) 144–156.
[24] J. Gil Sevillano, F. De las Cuevas, Scr. Mater. 66 (2012) 978–981.
[25] I. Gutierrez-Urrutia, D. Raabe, Acta Mater. 59 (2011) 6449–6462.
[26] D. Barbier, N. Gey, S. Allain, N. Bozzolo, M. Humbert, Mater. Sci. Eng. A 500 (2009) 196–206.
[27] I. Gutierrez-Urrutia, D. Raabe, Scr. Mater. 66 (2012) 992–996.
[28] D. Canadinc, H. Sehitoglu, H.J. Maier, Y.I. Chumlyakov, Acta Mater. 53 (2005) 1831.
[29] D. Raabe, Steel Res. 74 (2003) 327–337.
[30] Y. Su, Li Lin, R. Fu, J. Iron Steel Res. Int. 20 (2013) 46–53.
[31] D. Barbier, V. Favier, B. Bolle, Mater. Sci. Eng. A 540 (2012) 212–225.
[32] L. Meng, P. Yang, Q. Xie, h Ding, Z. Tang, Scr. Mater. 56 (2007) 931–934.
[33] R. Ueji, N. Tsuchida, D. Terada, N. Tsiju, Y. Tanaka, et al., Scr. Mater. 59 (2008) 963.
[34] K. Renard, P.J. Jacques, Mater. Sci. Eng. A 542 (2012) 8–14.
[35] J.A. Wollmershauser, B. Clausen, S.R. Agnew, Int. J. Fatigue 36 (2012) 181–193.
[36] X. Feaugas, Acta Mater. 47 (1999) 3617–3632.
[37] B. Peeters, S.R. Kalidindi, P. Van Houtte, E. Aernoudt, Acta Mater. 48 (2000) 2123–2133.
[38] Y. Estrin, H. Mecking, Acta Mater. 32 (1984) 57.
[39] H. Idrissi, K. Renard, L. Ryelandt, D. Schryvers, P.J. Jacques, Acta Mater. 58 (2010) 2464–2476.
[40] Z. Xu, N. Li, H. Jiang, L. Liu, Mater. Sci. Eng. A 621 (2015) 272–276.
[41] X.Z. Liao, Y.H. Zhao, S.G. Srinivasan, F. Zhou, Y.T. Zhu, R.Z. Valiev, D. V. Gunderov, Appl. Phys. Lett. 100 (2004) 592–594.
[42] L. Chen, H.S. Kim, S.K. Kim, B.C. De Cooman, ISIJ Int. 47 (2007) 1804.
[43] A. Rohatgi, K.S. Vecchio, G.T. Grey, Met. Mater. Trans. A 32 (2001) 135–168.

Please cite this article as: J.A. Benito, et al., Stress–strain response and microstructural evolution of a FeMnCAl TWIP steel during tension–compression tests, Materials Science & Engineering A (2016), http://dx.doi.org/10.1016/j.msea.2016.01.004